Steric Hindrance, Electronic Communication, and Energy Transfer in the Photo- and Electroluminescence Processes of Aggregation-Induced Emission Luminogens

Zujin Zhao,[‡] Shuming Chen,[‡] Jacky W. Y. Lam,[†] Cathy K. W. Jim,[†] Carrie Y. K. Chan,[†] Zhiming Wang,[§] Ping Lu,[†] Chunmei Deng,[†] Hoi Sing Kwok,[‡] Yuguang Ma,[§] and Ben Zhong Tang*[,†,‡,⊥]

Department of Chemistry, Institute of Molecular Functional Materials, Center for Display Research, The Hong Kong University of Science & Technology (HKUST), Clear Water Bay, Kowloon, Hong Kong, China, State Key Laboratory of Supramolecular Structure and Materials, Jilin University, Changchun 130012, China, and Department of Polymer Science and Engineering, Key Laboratory of Macromolecular Synthesis and Functionalization of the Ministry of Education of China, Zhejiang University, Hangzhou 310027, China

Received: November 11, 2009; Revised Manuscript Received: March 31, 2010

Methylpentaphenylsilole (MPPS) and tetraphenylethene (TPE) are two archetypal luminogens that show the novel effect of aggregation-induced emission (AIE). In this work, TPE moieties are attached to MPPS core as peripheral groups at 2,5- and 3,4-positions to generate new AIE luminogens. The resulting 2,5- and 3,4-BTPEMTPS adducts are weakly fluorescent in dilute solutions but become highly emissive as solid aggregates, verifying their AIE activities. Although weak in the absolute term, the emissions of the 2,5- and 3,4-BTPEMTPS luminogens are stronger than those of their parent forms of MPPS and TPE, due to the steric effect of the bulky TPE pedants on the intramolecular motions, especially the rotations of the phenyl rotors, in the BTPEMTPS systems. The emissions of 2,5-BTPEMTPS in the solution and aggregate states are more efficient and redder than those of 3,4-BTPEMTPS, revealing that the former is electronically more conjugated than the latter. Both the BTPEMTPS regioisomers are morphologically and thermally stable, showing high glass transition (T_g = 126 °C) and thermal-degradation temperatures (T_d up to 400 °C). The AIE luminogens serve as excellent emitters in electroluminescence (EL) devices, with maximum luminance up to 12560 cd/m^2. The EL deices using the blends of 2,5-BTPEMTPS and bis(tetraphenylethene) (BTPE) as emitting layers afford high current efficiencies (up to ∼7 cd/A) and external quantum efficiencies (up to ∼2.2%), thanks to the efficient energy transfer from the BTPE host to the 2,5-BTPEMTPS guest in the blending layer.

Introduction

Many conventional luminophores suffer from the notorious effect of aggregation-caused quenching (ACQ): their efficient luminescence processes in dilute solutions are often weakened or even totally exterminated when their molecules are aggregated, due to the formation of such detrimental species as excimers and exciplexes in the luminophore aggregates.[1] The ACQ effect has posed a thorny obstacle to the development of efficient light-emitting materials and devices in the solid state. Many research groups have taken various chemical, physical, and engineering approaches to hamper the formation of luminophore aggregates with the aim of mitigating the ACQ effect. Such efforts, however, have met with only limited success, because they are basically working against a natural process: it is well-known that luminophore molecules inherently aggregate in the condensed phase.[2]

We have recently discovered a novel phenomenon of aggregation-induced emission (AIE), which is exactly opposite to the ACQ effect discussed above.[3] In sharp contrast to the traditional luminophores, the AIE luminogens are nonemissive when dissolved in their good solvents but become highly emissive when aggregated in their poor solvents or in the solid state. 1-Methyl-1,2,3,4,5-pentaphenylsilole [MPPS (**1**); Chart 1] is the first luminogen that was found to show such an AIE effect in 2001.[4] Soon after that, AIE has been found to be a general effect observable in many luminogenic systems, especially in the luminogens with propeller-shaped molecular structures, such as 1,1,2,3,4,5-hexaphenylsilole [HPS (**2**)] and 1,1,2,2-tetraphenylethene [TPE (**3**)].[3,5−7] It has been rationalized that the AIE effect is caused by the restriction to intramolecular motions (RIM) in the luminogen aggregates.[5] In the dilute solutions, active intramolecular motions, especially the rotations of the multiple phenyl rotors against the silole or vinyl stator, efficiently deactivate the excited states of the luminogens in a nonradiative manner. In the solid state, however, the RIM process blocks the nonradiative relaxation channels and populates the radiative decays, thus making the luminogen aggregates highly luminescent.[3]

HPS and MPPS are the silole derivatives that emit strong green lights and show high electron mobility in the solid state.[8,9] The organic light-emitting diodes (OLEDs) fabricated from the silole derivatives have been found to show remarkably impressive performances, with device efficiencies up to theoretical limit.[8] TPE and its derivatives, on the other hand, have been extensively investigated as AIE-active blue light emitters, thanks to the simplicity in their syntheses and functionalizations.[3,6] It is envisioned that melding the silole and TPE units at the molecular level will generate new AIE luminogens with novel molecular structures and unique functional properties. In our previous work, we attempted to prepare a TPE-HPS adduct by

* To whom correspondence should be addressed. E-mail: tangbenz@ust.hk.
† Department of Chemistry, HKUST.
‡ Institute of Molecular Functional Materials, HKUST.
§ Jilin University.
⊥ Zhejiang University.

10.1021/jp910728x
Published on Web 04/12/2010

CHART 1: Structures of the AIE Luminogens Developed in Our Laboratories and Studied in This Work[a]

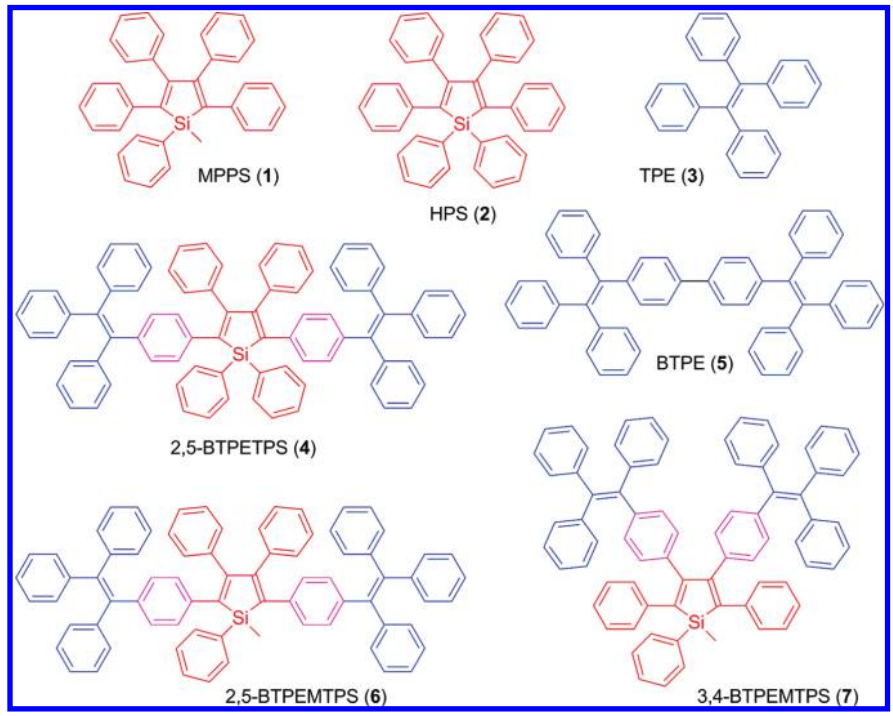

[a] Abbreviations: MPPS = 1-methyl-1,2,3,4,5-pentaphenylsilole (**1**), HPS = 1,1,2,3,4,5-hexaphenylsilole (**2**), TPE = 1,1,2,2-tetraphenylethene (**3**), 2,5-BTPETPS = 2,5-bis[4-(1,2,2-triphenylethenyl)phenyl]-1,1,3,4-tetraphenylsilole (**4**), BTPE = bis(tetraphenylethene) or 4,4′-bis(1,2,2-triphenylethenyl)biphenyl (**5**), 2,5-BTPEMTPS = 2,5-bis[4-(1,2,2-triphenylethenyl)phenyl]-1-methyl-1,3,4-triphenylsilole (**6**), and 3,4-BTPEMTPS = 3,4-bis[4-(1,2,2-triphenylethenyl)phenyl]-1-methyl-1,2,5-triphenylsilole (**7**).

cross-coupling of 2,5-metalated silole with brominated TPE but ended up with obtaining a homocoupling product of bis(tetraphenylethene) or BTPE (**5**), instead of the desired product of 2,5-BTPETPS (**4**).[10] The severe steric effect posed by the four phenyl rings attached to the silole core may have shielded the 2,5-positions, preventing the bulky TPE units from approaching the metalated reaction sites, leading to the failure in the synthesis of 2,5-BTPETPS.

The formation of the unexpected product of BTPE implies that its molecular structure is sterically less crowded. This reduced steric effect allows the BTPE molecules to undergo free intramolecular motions, especially twisting rotations, when they exist as isolated molecular species in their good solvents, as reflected by the practically nonluminescent nature and near-zero fluorescence quantum yield of BTPE in the solution state ($\Phi_{F,S} \rightarrow 0$).[10] In the aggregate state, however, the physical constraints among the condensed luminogen molecules activate the RIM process and make the BTPE solid highly luminescent, as evidenced by the high absolute fluorescence efficiencies of its thin film ($\Phi_{F,F} = 92\%$) and crystalline powder ($\Phi_{F,C} = 100\%$) measured by an integrating sphere. The low and high fluorescence efficiencies in the solution ($\Phi_{F,S}$) and aggregate ($\Phi_{F,A}$) states, respectively, endow BTPE with an extremely high AIE effect of $\alpha_{AIE} \rightarrow \infty$, where α_{AIE} is defined by the following equation:[10]

$$\alpha_{AIE} = \frac{\Phi_{F,A}}{\Phi_{F,S}} \quad (1)$$

While BTPE is a homoadduct of two TPE units, 2,5-BTPETPS is a cross-coupling product of two TPE pendants (BTPE) to an HPS core. Although we have failed to obtain 2,5-BTPETPS in our previous attempt, we are still interested in fusing TPE and silole units in a single molecular system. Taking into account that the severe steric effect has probably been the main cause for the synthetic failure in our previous work, in this study, we designed the molecular structures of two TPE-silole adducts somewhat less severe in the steric crowdedness. Specifically, we replaced a bulky phenyl ring in the 1-position of the silole core by a less bulky methyl group. This lessened steric effect enabled us to attach two TPE groups (BTPE) to a silole core at the 2,5- and 3,4-positions to furnish 2,5- (**6**) and 3,4-BTPEMTPS (**7**) luminogens, respectively (Schemes 1−3), using similar synthetic routes and experimental procedures to those employed in our previous work.[10]

Whereas BTPEMTPS experiences less steric effect than BTPETPS, it is sterically more crowded than BTPE. It was anticipated that BTPETPS would be luminescent in its solution, according to our proposed RIM mechanism for the AIE process,[3,5] but unfortunately, the steric effect in the cross-coupling reaction was too severe to allow it to be synthesized. In this regard, it is of great interest to compare the emission behaviors between BTPEMTPS and BTPE, because the comparison will offer mechanistic insight into the steric effects on the intramolecular motions and photophysical processes of the luminogens. In our previous study, we have studied photoluminescence (PL) behaviors of 1,1-substituted silole derivatives and found that the effect of 1,1-substituents is inductive in nature,[5] in agreement with the conclusions drawn from the studies conducted by other research groups.[12]

The 2,5- and 3,4-regioisomers of BTPEMTPS are expected to possess different extents of electronic conjugations and hence exhibit different PL properties. The electronic effect, however, has seldom been studied, mainly due to the involved synthetic difficulty.[12] The successful synthesis of the 2,5- and 3,4-BTPEMTPS luminogens in this work enabled us to investigate the electronic effects at the 2,5- and 3,4-positions on their light-

SCHEME 1: Preparation of Iodinated TPE Derivate (11)[a]

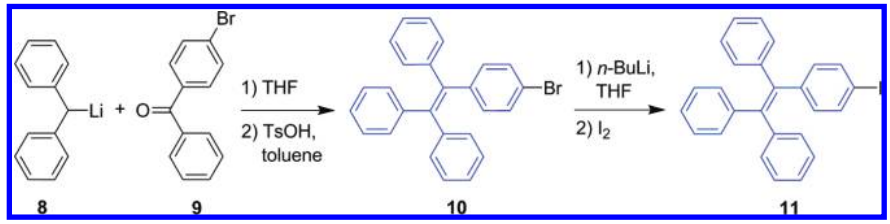

[a] Abbreviations: THF = tetrahydrofuran, TsOH = *p*-toluenesulfonic acid, and *n*-BuLi = *n*-butyllithium.

SCHEME 2: Synthesis of 2,5-BTPEMTPS (6) and BTPE (5)[a]

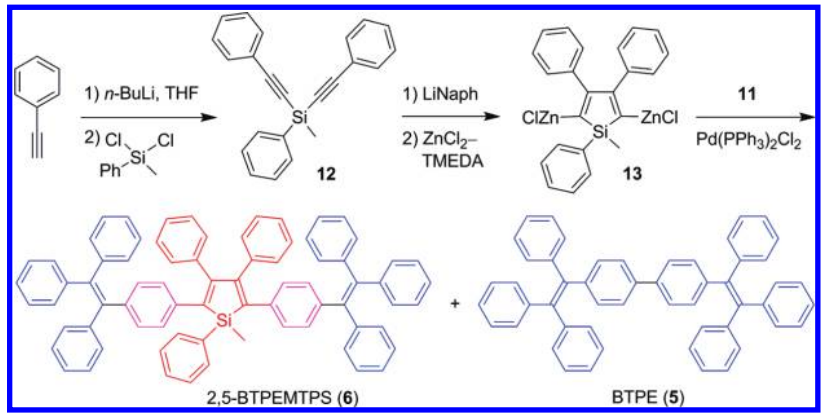

[a] Abbreviations: Ph = phenyl, Naph = naphthyl, and TMEDA = *N*,*N*,*N*′,*N*′-tetramethylenediamine.

emission processes. The BTPEMTPS luminogens were found to inherit the AIE activity from their TPE and silole parents and show high glass-transition and thermal-degradation temperatures. The strong emissions and high stabilities of the BTPEMTPS luminogens in the solid state allowed them to serve as active layers in the fabrication of efficient OLEDs.

Results and Discussion

Synthesis. The two new luminogens of 2,5- (**6**) and 3,4-BTPEMTPS (**7**) were prepared according to the synthetic routes shown in Schemes 1−3. 1-(4-Bromophenyl)-1-phenyl-2,2-diphenylethene (**10**) was prepared by the addition reaction of benzhydryllithium (**8**) with 4-bromobenzophenone (**9**) followed by the acid-catalyzed dehydration reaction. The brominated TPE derivate was then transformed to its more reactive iodinated congener (**11**) by the lithium-mediated halogen-exchange reaction. The 2,5-metalated silole intermediate (**13**) was prepared according to the experimental procedures reported in our previous paper with some modifications, using dichloro(methyl)(phenyl)silane, instead of dichlorodiphenylsilane, as a reactant.[10] The reduced steric effect in **13** and the enhanced reactivity of **11** enabled the synthesis of 2,5-BTPEMTPS (**6**) by the palladium-catalyzed cross-coupling reaction between **13** and **11** in a decent yield (41%), although the homocoupling product of BTPE (**5**) was still formed in the reaction.

Whereas the TPE units were incorporated into the silole structure at the late stage of the reactions in the synthesis of 2,5-BTPEMTPS (**6**), they were introduced into the silole skeleton at the early stage of the reactions in the preparation of its 3,4-regioisomer (**7**). The cross-coupling reaction between **17** and bromobenzene in the presence of the palladium catalyst afforded the desired product of 3,4-BTPEMTPS (Scheme 3). Although the steric effect involved in the coupling reaction was more severe than that in the synthesis of its 2,5-regioisomer, 3,4-BTPEMTPS was still obtained in a reasonable yield (34%). All the key intermediates and final products were carefully purified and fully characterized by the standard spectroscopic methods, from which satisfactory analysis data corresponding to their expected molecular structures were obtained (see the Experimental Section for detailed spectroscopic data). Both 2,5- and 3,4-BTPEMTPS are soluble in common organic solvents, such as THF, toluene, dichloromethane (DCM), and chloroform, but insoluble in water.

Photoluminescence. Figure 1 shows the absorption spectra of 2,5- and 3,4-BTPEMTPS luminogens in their dilute solutions in THF (10 μM). Whereas 3,4-BTPEMTPS exhibits an absorption peak at 325 nm, its 2,5-regioisomer shows a peak at a longer wavelength (395 nm) with a higher molar absorptivity (ε = 37 700 M^{-1} cm^{-1}). The red-shift in the absorption peak and the increase in the molar absorptivity indicate that the 2,5-BTPEMTPS luminogen is more conjugated than its 3,4-regioisomer, due to the better electronic communication of the TPE peripheral units at the 2,5-positions with the central silole ring. From the onsets of the absorption spectra, the band gaps of 2,5- and 3,4-BTPEMTPS luminogens are estimated to be 2.7 and 3.1 eV, respectively (Table 1).

The PL spectra of the 2,5- and 3,4-BTPEMTPS luminogens in the dilute THF solutions are weak in intensity, showing emission maxima at 520 and 490 nm, respectively. The Φ_F values for 2,5- and 3,4-BTPEMTPS estimated with use of 9,10-diphenylanthrance as standard are 0.34% and 0.38%, respectively, indicating that they are weak emitters when molecularly dissolved in their good solvents. When a large amount of nonsolvent, such as water, is added into their THF solutions, intense PL spectra are recorded under identical measurement conditions. Figure 2A shows the PL spectra of 2,5-BTPEMTPS in pure THF and THF/water mixtures. The emission remains weak when up to 70% of water is added into THF; afterward, it starts to increase swiftly (Figure 2B). Similar results are obtained for 3,4-BTPEMTPS: it is weakly luminescent when dissolved in THF but becomes highly emissive when aggregated in the THF/water mixtures with high water contents (f_w > 70%).

SCHEME 3: Synthesis of 3,4-BTPEMTPS (7)

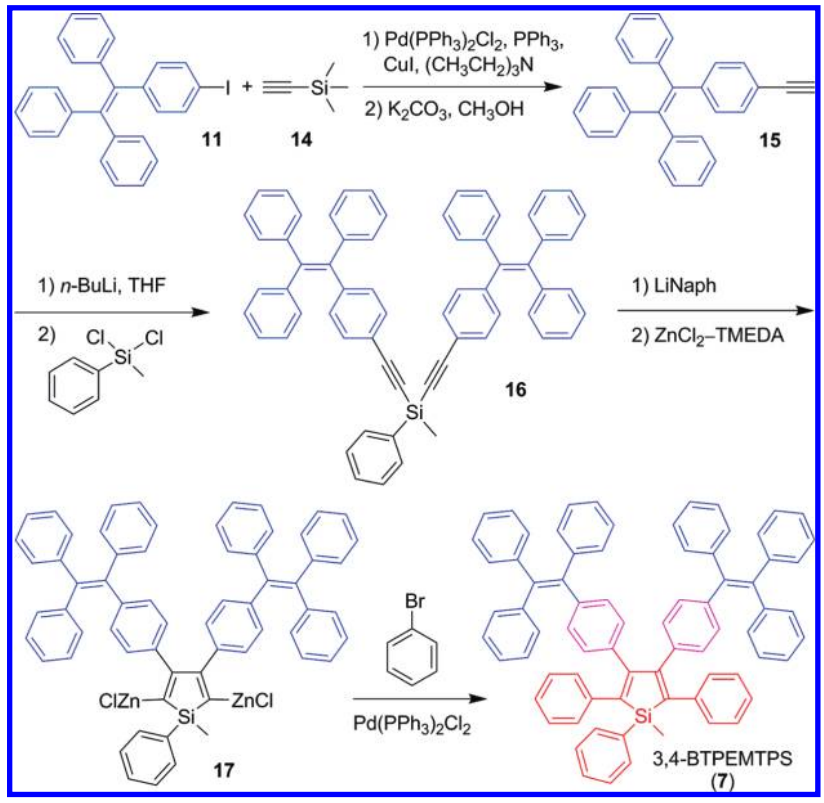

Evidently, like their silole and TPE parents, the 2,5- and 3,4-BTPEMTPS luminogens are AIE-active.

While the emission efficiencies of the 2,5- and 3,4-BTPEMTPS solutions are low in absolute terms ($\Phi_F = 0.34-0.38\%$), in relative terms they are higher than those of their parent forms of TPE ($\Phi_F = 0.24\%$) and MPPS ($\Phi_F = 0.09\%$)[5a,13] as well as their congener of BTPE ($\Phi_F \approx 0\%$; Table 1).[10] In the solutions of TPE and MPPS, the active intramolecular rotations of their phenyl rotors nonradiatively deactivate their excitons, making them weakly luminescent in the solution state. The almost unrestricted intramolecular rotations of the multiple phenyl rotors in BTPE further aggravate the effect and totally quench its PL process. The steric effect in 2,5-BTPEMTPS, however, makes its phenyl rotors less free to undergo the intramolecular rotations and as a result its Φ_F is slightly increased.[5b] As discussed above, the steric effect in 3,4-BTPEMTPS is more severe than that in its 2,5-regioisomer, hence the further enhanced Φ_F value for the 3,4-regioisomer. The steric effect observed here is in agreement with that found in a recent study, where a TPE core decorated by four bulky 1,2,3,4,5,6-hexaphenylbenzene (HPB) units at 1,1,2,2-positions was found to show a Φ_F value of 13%, because of the very severe steric effect of the HPB substituents on the intramolecular rotations of the phenyl rotors of the TPE derivative.[14]

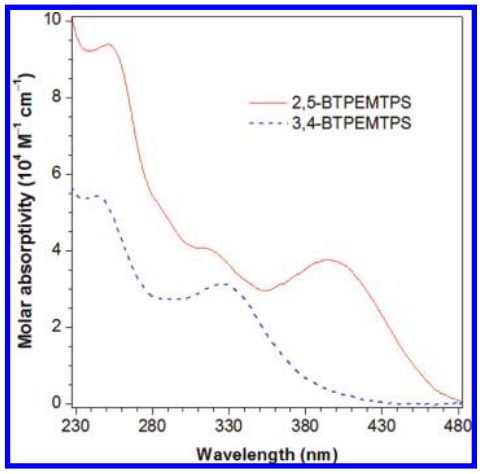

Figure 1. Absorption spectra of THF solutions of 2,5- and 3,4-BTPEMTPS.

We further investigated PL behaviors of amorphous films of 2,5- and 3,4-BTPEMTPS luminogens. The emission of the 2,5-BTPEMTPS film is peaked at 535 nm, which is 35 nm bathochromically shifted from that of its 3,4-congener, due to the better electronic conjugation in the 2,5-regioisomer (Figure 3A). In sharp contrast to their weak fluorescence in the solution state, both 2,5- and 3,4-BTPEMTPS luminogens emit strongly in the condensed phase with Φ_F values (measured by an integrating sphere) of 51.2% and 46.9%, respectively (Table 1). The α_{AIE} values (defined as the ratios of $\Phi_{F,F}/\Phi_{F,S}$) for the 2,5- and 3,4-BTPEMTPS luminogens are 151 and 123, respectively, which are smaller than those for their parent forms of TPE (205) and MPPS (944). The steric hindrance in the BTPEMTPS luminogens makes their phenyl rotors less free to undergo intramolecular rotations and hence makes their solutions more fluorescent. It is this enhanced emission in the solution state that has mainly contributed to the observed decreases in the α_{AIE} values of the BTPEMTPS luminogens.

To better understand the photophysical properties of the 2,5- and 3,4-BTPEMTPS luminogens, we performed theoretical calculations on their energy levels. Their HOMO and LUMO plots are given in Figure 4. The HOMO and LUMO of 2,5-BTPEMTPS are dominated by the orbitals from the central silole ring and the two peripheral TPE units at the 2,5-postions, whereas the phenyl rings at the 3,4- and 1-positions are twisted out of the plane of the silole core, thus contributing little to the energy levels of the luminogen. This orbital distribution results

TABLE 1: Optical and Thermal Properties of TPE and Silole Derivatives[a]

AIE luminogen[b]	λ_{ab} (nm)	λ_{em} (nm) soln	aggr	cryst	amor	$\Phi_{F,S}$ (%)	$\Phi_{F,F}$ (%)	α_{AIE}	E_g (eV)	T_g (°C)	T_d (°C)
2,5-BTPEMTPS (**6**)	395	520	532		535	0.34	51.2	150.6	2.7	126	400
3,4-BTPEMTPS (**7**)	325	490	495		500	0.38	46.9	123.4	3.1		360
BTPE (**5**)	340		483	445	499	~0	92.0	∞	3.1	221	368
TPE (**3**)	299		462	440	475	0.24	49.2	205.0	3.5		224
MPPS (**1**)	363	491	494		491	0.09	85.0	944.4	2.9	54	309
HPS (**2**)	366	497	499		495	0.10	78.0	780.0	2.9	65	351

[a] Abbreviations: soln = solution (in THF, c = 10 μM), aggr = aggregate, cryst = crystalline, amor = amorphous, λ_{ab} = maximum absorption wavelength (in THF), λ_{em} = maximum emission wavelength, $\Phi_{F,S}$ = fluorescence quantum yield for THF solution estimated with use of 9,10-diphenylanthracene (Φ_F = 90% in cyclohexane) as standard, $\Phi_{F,F}$ = fluorescence quantum yield for thin film determined by an integrating sphere, α_{AIE} = extent of emission enhancement ($\Phi_{F,F}/\Phi_{F,S}$) or AIE effect, E_g = energy band gap estimated from the onset of absorption spectrum, T_g = glass-transition temperature, and T_d = onset decomposition temperature. [b] Data for BTPE, TPE, MPPS, and HPS taken from refs 10, 6, 5a and 13, respectively.

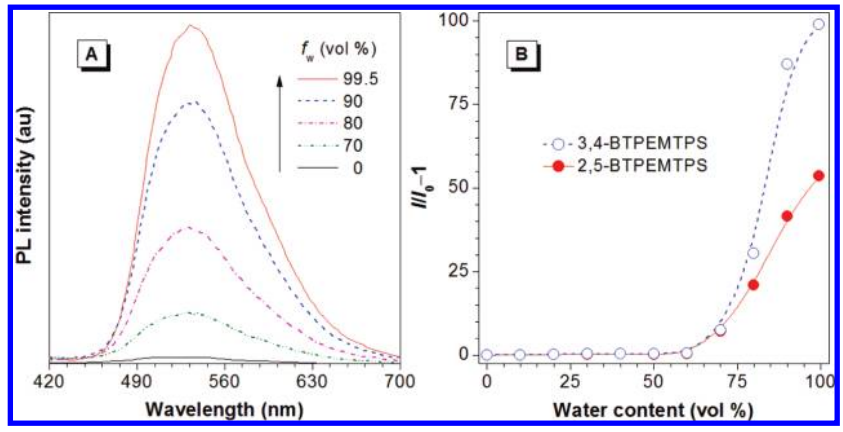

Figure 2. (A) Emission spectra of 2,5-BTPEMTPS in THF/water mixtures with different water contents (f_w). (B) Plots of $I/I_0 - 1$ versus f_w for 2,5- and 3,4-BTPEMTPS in the aqueous mixtures, where I_0 is the PL intensity in the pure THF solution. Luminogen concentration: 10 μM; excitation wavelength: 350 nm.

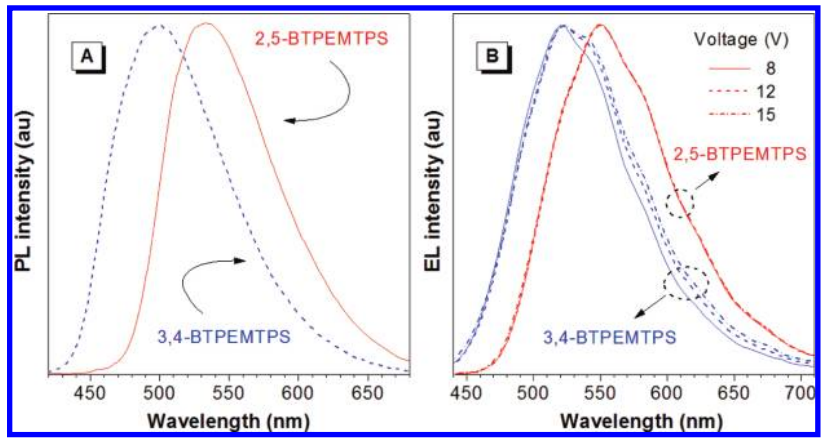

Figure 3. (A) PL spectra of amorphous films of 2,5- and 3,4-BTPEMTPS. (B) EL spectra of 2,5- and 3,4-BTPEMTPS in multilayer OLEDs with a device configuration ITO/NPB/BTEMTPS/TPBi/LiF/Al.

in a linear and extended conjugation in 2,5-BTPEMTPS. The two peripheral TPE units are also conjugated with the central silole ring in 3,4-BTPEMTPS. The orbitals of its HOMO and LUMO, however, are distributed in an X-shaped manner, which has somehow shortened its effective conjugation length. The calculated energy band gap for 2,5-BTPEMTPS is 3.24 eV, which is narrower than that for its 3,4-regioisomer (3.44 eV). The trend is the same as that of the experimental data (cf., Table 1), though the calculated values are somewhat higher than the experimental ones. The theoretical study nicely explains the bathochromic shifts in the absorption and emission of 2,5-BTPEMTPS from those of its 3,4-regioisomer.

Stability. Thermal transitions and stabilities of the BTPEMTPS luminogens were investigated by thermogravimetric analysis (TGA) and differential scanning calorimetry (DSC) in an atmosphere of dry nitrogen. As can be seen from Figure 5, the 2,5- and 3,4-BTPEMTPS luminogens commence to lose their weights at temperatures (T_d) of 400 and 360 °C, respectively. From the DSC thermogram shown in the inset of Figure 5, a glass-transition temperature (T_g) of 126 °C is readily identified. No glass transition process was detected in the case of the 3,4-BTPEMTPS luminogen, although its sample had been carefully scanned several times.

The T_d values of the BTPEMTPS luminogens are much higher than those of their parent forms of TPE (224 °C) and MPPS (309 °C; cf., Table 1). The T_g value of 2,5-BTPEMTPS is more than 2-fold higher than that of MPPS (54 °C). These thermal analysis data indicate that the BTPEMTPS luminogens are

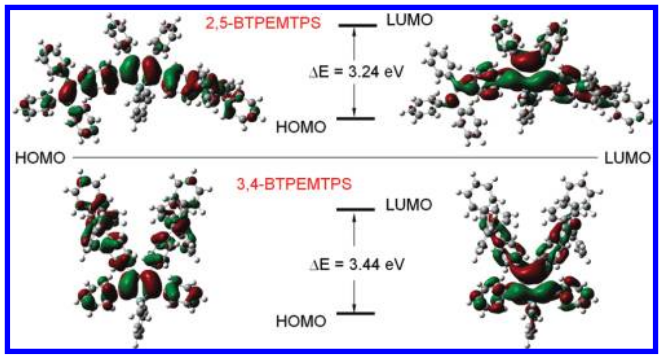

Figure 4. Molecular orbital amplitude plots of HOMO and LUMO energy levels of (upper panel) 2,5- and (lower panel) 3,4-BTPEMTPS luminogens calculated with use of the B3LYP/6-31G(d) basis set.

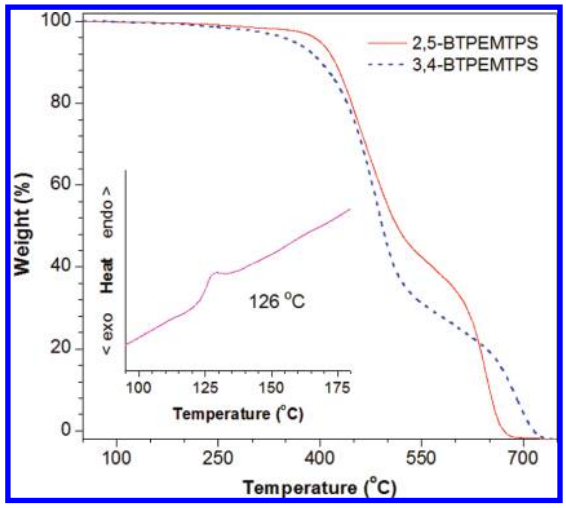

Figure 5. TGA thermograms of 2,5- and 3,4-BTPEMTPS luminogens recorded under nitrogen at a heating rate of 10 deg/min. Inset: DSC curve of 2,5-BTPEMTPS recorded during the second heating scan.

thermally and morphologically stable. The high stabilities of the luminogens, along with their efficient solid-state emissions, make them promising for high-tech applications, especially as emitting materials in the construction of OLED devices.

Electroluminescence. We fabricated multilayer OLEDs with a device configuration of ITO/NPB (60 nm)/BTPEMTPS (40 nm)/TPBi (20 nm)/LiF (1 nm)/Al (100 nm), in which BTPMTPS, NPB, and TPBi functioned as light-emitting, hole-transport, and electron-transport (or hole-blocking) layers, respectively (Figure 6). The EL spectrum of the OLED based on 3,4-BTPEMTPS is peaked at 520 nm and changes little with the applied voltage (Figure 3B). Owing to its better electronic conjugation, the OLED based on 2,5-BTPEMTPS emits at 552 nm, which is 32 nm red-shifted from that of its 3,4-regioisomer. The OLED of 2,5-BTPEMTPS enjoys outstanding spectral stability, with no spectral change observed at all when the applied voltage was changed from 8 to 15 V. The EL spectra of the BTPEMTPS luminogens are located in the longer wavelength region, in comparison to their PL spectra, probably due to the microcavity effect and the formation of exciplexes or electroplexes between light-emitting and charge-transport layers.[15]

Figure 7 shows the changes in the current density, luminance (L), and current efficiency (η_C) of the BTPEMTPS-based OLEDs with applied voltage. The EL device of 3,4-BTPEMTPS is turned on at a voltage (V_{on}) of 6.2 V. The EL intensity is increased with an increase in the applied voltage, with the luminance reaching 3980 cd/m^2 at 15 V. The maximum current efficiency ($\eta_{C,max}$), power efficiency ($\eta_{P,max}$), and external

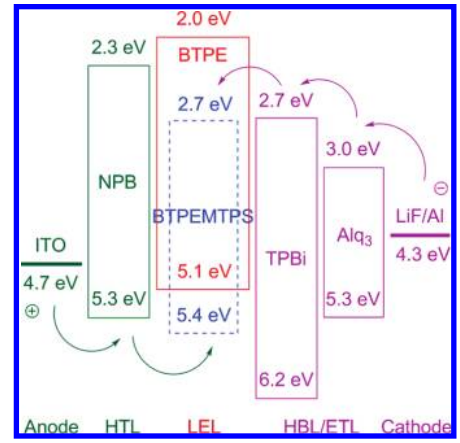

Figure 6. Energy level diagram for the multilayer OLED with a device configuration of ITO/NPB/LEL/TPBi/(Alq$_3$/)LiF/Al, where ITO = indium tin oxide, NPB = *N*,*N*-bis(1-naphthyl)-*N*,*N*-diphenylbenzidine, HTL = hole-transport layer, LEL = light-emitting layer (BTPEMTPS or BTPE or BTPEMTPS:BTPE), TPBi = 2,2′,2″-(1,3,5-benzinetriyl)-tris(1-phenyl-1*H*-benzimidazole), HBL = hole-blocking layer, ETL = electron-transport layer, and Alq$_3$ = tris(8-hydroxyquinolinolato)aluminum.

quantum efficiency ($\eta_{ext,max}$) of the OLED are 4.96 cd/A, 2.05 lm/W, and 1.66%, respectively (Table 2, no. 1). The OLED device based on 2,5-BTPEMTPS starts to emit a yellow light at a lower voltage (V_{on} = 5.2 V) and furnishes a higher maximum luminance (L_{max} = 12560 cd/m^2), in comparison to the device of its 3,4-regioisomer. The $\eta_{C,max}$, $\eta_{P,max}$, and $\eta_{ext,max}$ values attained by the EL device of 2,5-BTPEMTPS are all higher, being 6.40 cd/A, 2.45 lm/W, and 1.98%, respectively (Table 2, no. 2). Evidently, the attachment of the TPE peripheral units to the 2,5-positions of the silole core has resulted in a luminogen with better EL performances. In other words, the device performances of the OLED based on BTPEMTPS can be tuned by changing the regiostructure of the emitter.

BTPE, the byproduct obtained in the synthesis of 2,5-BTPEMTPS (cf., Scheme 2), is also AIE-active and emits intensely in the condensed phase.[10] Figure 8A shows the PL and EL spectra of BTPE as well as the absorption spectrum of 2,5-BTPEMTPS. The amorphous film of BTPE emits at 499 nm in a high efficiency (Φ_F = 92%), while the emission of its crystalline powder is peaked at 445 nm with an absolute Φ_F value of 100%, which is 54 nm blue-shifted in emission color and ~1.1-fold enhanced in emission efficiency from the PL of its amorphous-film counterpart. The blue-shift and intensity-enhancement in the PL of crystalline powder from that of amorphous film are a general phenomenon often observed in many AIE luminogen systems.[3] The efficient solid-state PL enables BTPE to serve as an excellent light-emitting material for the construction of EL devices. The OLED utilizing BTPE as the light-emitting layer shows an EL spectrum peaked at 488 nm, locating between the PL spectra of its amorphous film and that of its crystalline powder. This implies that the BTPE layer in the device is semicrystalline in morphology. The OLED is efficient, affording a luminance as high as 11180 cd/m^2 and EL efficiencies as high as 7.26 cd/A and 3.17% (Table 2, no. 3).[10]

As can be seen from Figure 8A, the emission spectra of BTPE partially overlap with the absorption spectrum of 2,5-BTPEMTPS. The energy transfer from BTPE to 2,5-BTPEMTPS may allow the former to function as a host material in a blending OLED with the latter working as a guest material. We thus fabricated OLEDs with a device structure of ITO/NPB

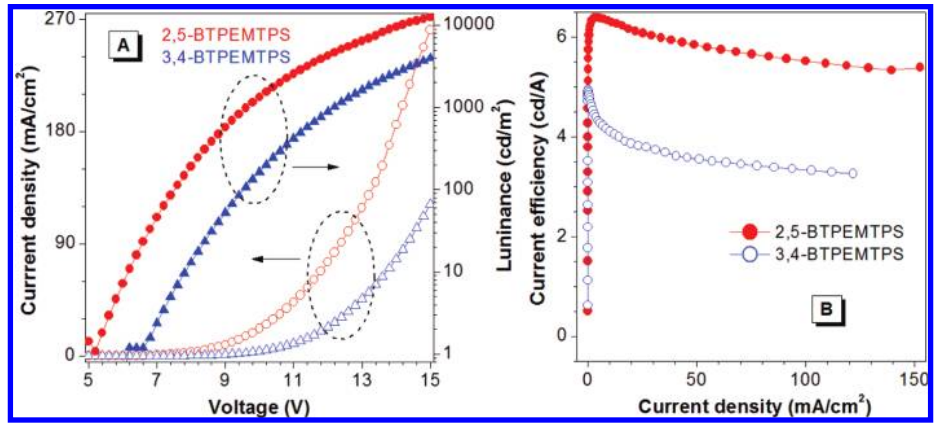

Figure 7. (A) Changes in current density and luminance with applied voltage and (B) plots of current efficiency versus current density in the multilayer OLEDs with a device configuration of ITO/NPB/BTPEMTPS/TPBi/LiF/Al.

TABLE 2: Performances of OLEDs Based on BTPE, BTPEMTPS, and Their Blends[a]

no.	active layer	λ_{EL} (nm)	V_{on} (V)	L_{max} (cd/m^2)	$\eta_{P,max}$ (lm/W)	$\eta_{C,max}$ (cd/A)	$\eta_{ext,max}$ (%)
1	3,4-BTPEMTPS	520	6.2	3980	2.05	4.96	1.66
2	2,5-BTPEMTPS	552	5.2	12560	2.45	6.40	1.98
3	BTPE	488	4.0	11180	3.81	7.26	3.17
4	2,5-BTPEMTPS(10 wt %):BTPE	540	4.8	8894	3.36	6.64	2.13
5	2,5-BTPEMTPS(20 wt %):BTPE	544	4.6	10480	3.24	7.02	2.18

[a] Device configurations: ITO/NPB (60 nm)/BTPEMTPS (40 nm)/TPBi (20 nm)/LiF (1 nm)/Al (100 nm) (for nos. 1 and 2), ITO/NPB (60 nm)/BTPE (20 nm)/TPBi (10 nm)/Alq_3 (30 nm)/LiF (1 nm)/Al (100 nm) (for no. 3), and ITO/NPB (60 nm)/BTPEMTPS:BTPE (20 nm)/TPBi (10 nm)/Alq_3 (30 nm)/LiF (1 nm)/Al (100 nm) (for nos. 4−6). Abbreviations: λ_{EL} = maximum emission wavelength, V_{on} = turn-on voltage (at 1 cd/m^2), L_{max} = maximum luminance (at 15 V), $\eta_{P,max}$ = maximum power efficiency, $\eta_{C,max}$ = maximum current efficiency, and $\eta_{ext,max}$ = maximum external quantum efficiency.

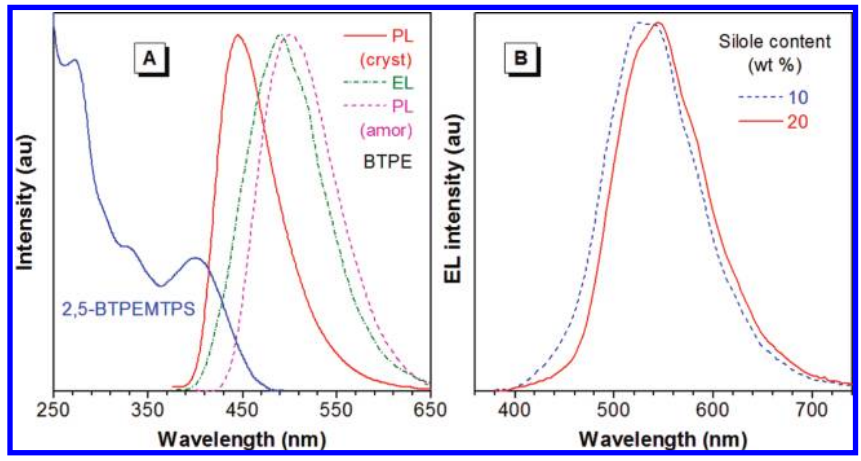

Figure 8. (A) Absorption spectrum of 2,5-BTPEMTPS and emission (PL and EL) spectra of BTPE in the crystalline (cryst) and amorphous (amor) phases; device configuration of the BTPE-based OLED: ITO/NPB/BTPE/TPBi/Alq_3/LiF/Al. (B) EL spectra of OLEDs based on 2,5-BTPEMTPS:BTPE blends with different silole contents; device configuration: ITO/NPB/2,5-BTPEMTPS:BTPE/TPBi/Alq_3/LiF/Al.

(60 nm)/2,5-BTPEMTPS:BTPE (20 nm)/TPBi (10 nm)/Alq_3 (30 nm)/LiF (1 nm)/Al (100 nm) (cf., Figure 6 and Table 2). The OLED configuration is the same as that of BTPE, except for the pure BTPE layer being replaced by a layer of blending film of 2,5-BTPEMTPS:BTPE, with a silole content of 10% or 20%. The EL peak of the BTPE host is absent in the EL spectra of the blending OLEDs (Figure 8B), indicative of an efficient energy transfer from the BTPE host to the 2,5-BTPEMTPS guest in the emitting layer. The device performances of the blending OLEDs are shown in Figure 9. With an increase in the BTPEMTPS content in the blending-film layer, the turn-on voltage is decreased, whereas the current density, luminance, and current efficiency are all increased.

Internal quantum efficiency (η_{int}) of an EL device with singlet excitons as emitting species is known to be determined by the product of the PL quantum efficiency of the light-emitting material (Φ_F), the electroexcitation efficiency (γ_{EL}), and the efficiency or probability of the formation of singlet excitons (η_r):

$$\eta_{int} = \Phi_F \gamma_{EL} \eta_r \quad (2)$$

where γ_{EL} is defined as the ratio of the number of exciton formation events to the number of electrons flowing in the external circuit or the probability of carrier recombination with formation of excitons, and η_r is defined as the ratio of the number of singlet excitons to the total number of excitons including both singlet and triplet excitons, also known as singlet to triplet branching ratio. The η_{ext} of an OLED device is the product of its η_{int} and the light output coupling factor (β):

$$\eta_{ext} = \beta\eta_{int} = \frac{1}{2n^2}\Phi_F\gamma_{EL}\eta_r \quad (3)$$

Since n (refractive index) is a constant for a given material and η_r is also a constant (25%) according to the spin statistics, eq 3 can be rewritten as follows:

$$\eta_{ext} = c\Phi_F\gamma_{EL} \quad (4)$$

where c is a constant that equals $\eta_r/2n^2$. In other words, η_{ext} is determined by the product of the PL efficiency and the probability of the carrier recombination that leads to exciton formation.

The energy diagram shown in Figure 6 suggests that the hole- and electron-injections into the emitting layer from the NPB and TPBi layers, respectively, are more efficient in the OLED based on BTPEMTPS, in comparison to that of BTPE. Experimentally, however, the BTPE device shows better performance than the BTPEMTPS device, with the former being 1.6-fold higher than the latter (cf., Table 2). This implies that the PL efficiency has played a predominant role in the EL process, taking into consideration that the $\Phi_{F,F}$ value of the BTPE film is 1.8-fold higher than that of the 2,5-BTPEMTPS film (cf., Table 2). The performance of the BTPEMTPS-based EL device is enhanced by simply introducing BTPE into the emitting layer as a host, taking advantage of its high PL quantum efficiency as well as the efficient energy transfer from the host to the guest.

Conclusion

In summary, in this work, a synthetic route was elaborated to enable the meld of TPE and silole units at the molecular level and the resulting regioisomers of BTPEMTPS afforded a platform for studying the steric and electronic effects on their emission behaviors in the solution and solid states. The steric effect in the BTPEMTPS luminogens makes their phenyl rotors less free to undergo intramolecular motions. As a result, their solution emissions become more intense than those of their parent forms, although the $\Phi_{F,S}$ values of the BTPEMTPS luminogens remain low in absolute terms. The fluorescence of 2,5-BTPEMTPS is red-shifted from that of its 3,4-regioisomer, due to the more conjugated electronic structure of the former than the latter. The AIE luminogens are thermally and morphologically stable. The OLED based on 2,5-BTPEMTPS shows better device performance than that of its 3,4-isomer. The EL efficiency of the silole-based OLED is further enhanced by using a blending film of 2,5-BTPEMTPS and BTPE as emitting layer, thanks to the efficient energy transfer from the BTPE host to the silole guest.

Experimental Section

General Information. THF was distilled from sodium benzophenone ketyl in an atmosphere of dry nitrogen immediately prior to use. Methylphenylbis(phenylethynyl)silane (**12**) was prepared according to our previously published experimental procedures.[16] All other chemicals and regents were purchased from Aldrich and used as received without further purification.

^{1}H and ^{13}C NMR spectra were measured on a Bruker AV 300 spectrometer in deuterated chloroform or DCM with tetramethylsilane (TMS; $\delta = 0$) as internal reference. Absorption spectra were taken on a Milton Roy Spectronic 3000 Array spectrophotometer. Emission spectra were recorded on a Perkin-Elmer LS 55 spectrofluorometer. MALDI-TOF mass spectrum was taken on a GCT premier CAB048 mass spectrometer.

Cyclic voltammetry curves were recorded on a Princeton Applied Research potentiostat (model 273A). All the electrochemical measurements were carried out at room temperature with use of a conventional three-electrode configuration in distilled DCM, using Bu_4NPF_6 (0.1 M) as the supporting electrolyte. The working and reference electrodes were glassy carbon and $Ag/AgNO_3$ (0.1 M in acetonitrile), respectively. The reference electrode was checked versus ferrocene as recommended by IUPAC. All the solutions were deaerated by bubbling nitrogen gas for a few minutes prior to the electrochemical measurements.

Elemental analysis was performed on an Elementary Vario EL analyzer. TGA was carried out on a TA TGA Q5000 under dry nitrogen at a heating rate of 10 deg/min. Thermal transitions were investigated by DSC, using a TA DSC Q1000 under dry nitrogen at a heating rate of 10 deg/min. The X-ray diffraction diagram was recorded on a Philips PW 1830 powder diffractometer, using the monochromatized X-ray beam from nicked-filtered Cu Kα radiation ($\lambda = 1.5406$ Å).

Luminogen Synthesis. The AIE luminogens were prepared according to the synthetic routes shown in Schemes 1−3. The detailed experimental procedures for the syntheses of the key intermediates and final products and their characterization data are given below.

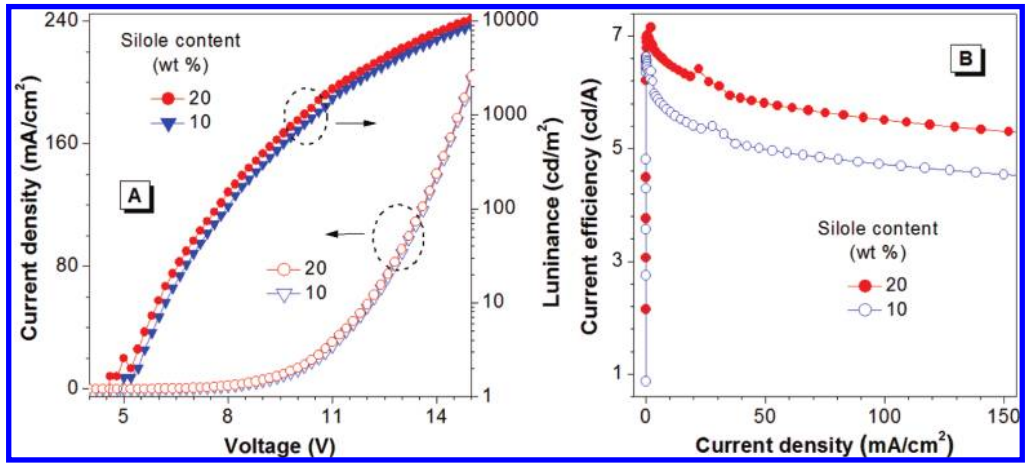

Figure 9. (A) Changes in current density and luminance with applied voltage and (B) plots of current efficiency versus current density in the multilayer OLEDs with a device configuration of ITO/NPB/2,5-BTPEMTPS:BTPE/TPBi/Alq_3/LiF/Al.

1-(4-Bromophenyl)-1,2,2-triphenylethene (10). *n*-Butyllithium (1.6 M in hexane, 7.5 mL, 12 mmol) was added dropwise to a solution of diphenylmethane (2.02 g, 12 mmol) in dry THF (50 mL) at 0 °C under nitrogen. The resulting orange-red solution was stirred for 1 h at 0 °C and then transferred slowly to a solution of 4-bromobenzophenone (**9**; 2.6 g, 10 mmol) in THF (20 mL) at 0 °C. The mixture was allowed to warm to room temperature and stirred for 6 h. The reaction was quenched by adding an aqueous solution of ammonium chloride into the mixture. The organic layer was extracted with DCM. The combined organic layers were washed with a saturated brine solution and dried over anhydrous magnesium sulfate. After filtration and evaporation, the resulting crude alcohol product (containing excess diphenylmethane) was dissolved in ~80 mL of toluene, into which a catalytic amount of TsOH (0.5 g, 2.6 mmol) was added. After being refluxed for 6 h, the mixture was cooled to room temperature, washed with a saturated brine solution, and dried over anhydrous magnesium sulfate. After filtration and solvent evaporation, the residue was purified by silica gel column chromatography with *n*-hexane as eluent. **10** was obtained as a white solid in 86% yield (3.5 g).

^{1}H NMR (300 MHz, CD_2Cl_2): δ (TMS, ppm) 7.20 (d, 2H, J = 6.0 Hz), 7.12−7.07 (m, 9H), 7.02−6.98 (m, 6H), 6.88 (d, 2H, J = 6.3 Hz). ^{13}C NMR (75 MHz, CD_2Cl_2): δ (TMS, ppm) 143.37, 143.28, 143.18, 142.66, 141.55, 139.61, 132.94, 131.26, 131.20, 131.18, 130.81, 127.84, 127.74, 127.64, 126.66, 126.61, 126.55, 120.40. HRMS: m/z 412.0680 (M^+, calcd 412.0650).

1-(4-Ethynylphenyl)-1,1,2-triphenylethene (15). *n*-Butyllithium (1.6 M in hexane, 3.8 mL, 6 mmol) was added dropwise into a THF solution (50 mL) of **10** (2 g, 5 mmol) at −78 °C. After the solution was stirred for 3 h, iodine (1.4 g, 5.5 mmol) was added into the solution in three portions. After being warmed to room temperature and stirred for 2 h, the mixture was poured into water and extracted with DCM. The organic layer was washed by saturated sodium thiosulfate solution and water, then dried over magnesium sulfate. After filtration and solvent evaporation, the crude product **11** was dried under vacuum to a constant weight.

The dried product **11** was added into a mixture of trimethylsilylacetylene (0.6 g, 6 mmol), copper(I) iodide (20 mg, 0.1 mmol), $Pd(PPh_3)_2Cl_2$ (11.5 mg, 0.01 mmol), and triphenylphosphine (10.5 mg, 0.04 mmol) in dry triethylamine (150 mL). After the solution was purged with nitrogen for half an hour, the reaction was refluxed under nitrogen for 12 h. The solution was then cooled to room temperature. After solvent evaporation, the mixture was subjected to shot flash column chromatography. The resulting crude product was added into a methanol solution (80 mL) of potassium carbonate (1.5 g). The reaction was stirred overnight at room temperature. The mixture was poured into water and extracted with DCM. The organic layer was washed with water and dried over magnesium sulfate. After filtration and solvent evaporation, the residue was purified by silica gel column chromatography, using *n*-hexane/DCM as eluent. **15** was obtained as a white solid in 78% yield (1.4 g).

^{1}H NMR (300 MHz, $CDCl_3$): δ (TMS, ppm) 7.22 (d, 2H, J = 8.4 Hz), 7.13−7.09 (m, 9H), 7.03−7.00 (m, 8H). ^{13}C NMR (75 MHz, $CDCl_3$): δ (TMS, ppm) 144.6, 143.5, 143.4, 143.3, 141.9, 140.2, 131.6, 131.4, 131.3, 127.9, 127.8, 127.7, 126.8, 126.7, 119.9, 83.9. HRMS: m/z 356.1541 (M^+, calcd 356.1565).

Methyl(phenyl)bis{[4-(1,2,2-triphenylvinyl)phenyl]ethynyl}-silane (16). *n*-Butyllithium (1.6 M in hexane, 3.8 mL, 6 mmol) was added dropwise into a solution of **15** (1.8 g, mmol) in dry THF (50 mL) at −78 °C. After the mixture was stirred at −78 °C for 3 h, dichloro(methyl)(phenyl)silane (0.46 g, 2.4 mmol) was added. The mixture was then warmed to room temperature and stirred for an additional 6 h. The reaction was terminated by adding hydrochloric acid (2 M, 10 mL). The mixture was poured into water and then extracted with DCM. The organic layer was washed with water and dried over magnesium sulfate. After filtration and solvent evaporation, the residue was purified by silica gel column chromatography, using *n*-hexane/DCM as eluent. **4** was obtained as a white solid in 86% yield (1.7 g).

^{1}H NMR (300 MHz, CD_2Cl_2): δ (TMS, ppm) 7.78−7.75 (m, 2H), 7.41−7.39 (m, 3H), 7.25 (d, 4H, J = 8.4 Hz), 7.13−7.07 (m, 18H), 7.03−6.97 (m, 16H). ^{13}C NMR (75 MHz, CD_2Cl_2): δ (TMS, ppm) 145.7, 144.2, 144.1, 144.0, 142.7, 140.9, 134.8, 132.2, 132.0, 131.9, 130.9, 128.8, 128.6, 128.5, 128.4, 127.5, 127.4, 120.9, 108.2, 89.8, 0.5. HRMS: m/z 830.3307 (M^+, calcd 830.3369).

2,5-BTPEMTPS (6). A solution of lithium 1-naphthalenide (LiNaph) was prepared by stirring a mixture of 1-naphthalene (2.56 g, 20 mmol) and lithium granular (0.14 g, 20 mmol) in dry THF (30 mL) for 12 h at room temperature under nitrogen. A solution of **12** (1.6 g, 5 mmol) in THF (20 mL) was then added dropwise into the solution of LiNaph, and the resulting reaction mixture was stirred for 1 h at room temperature. After the solution was cooled to −10 °C, $ZnCl_2$-TMEDA (6.3 g, 25 mmol) and 20 mL of THF were added. The fine suspension was stirred for 1 h at room temperature and $Pd(PPh_3)_2Cl_2$ (100 mg), **11** (4.1 g, 10 mmol), and 10 mL of THF were then added. After being refluxed for 12 h, the mixture was cooled to room temperature and the reaction was terminated by the addition of 2 M hydrochloric acid. The mixture was poured into water and extracted with DCM. The organic layer was washed successively with aqueous sodium chloride solution and water and then dried over magnesium sulfate. After filtration, the solvent was evaporated under reduced pressure and the residue was purified by silica gel column chromatography, using *n*-hexane/DCM as eluent followed by recrystallization.2,5-BTPEMTPS was obtained as a yellow solid in 41% yield based on the amount of **12** used.

^{1}H NMR (300 MHz, CD_2Cl_2): δ (TMS, ppm) 7.57 (d, 2H, J = 6.6 Hz), 7.40−7.31 (m, 3H), 7.06−7.00 (m, 24H), 6.95−6.92 (m, 8H), 6.89−6.86 (m, 4H), 6.82−6.79 (m, 4H), 6.63 (d, 4H, J = 8.4 Hz), 6.54 (d, 4H, J = 8.7 Hz), 0.69 (s, 3H). ^{13}C NMR (75 MHz, $CDCl_3$): δ (TMS, ppm) 156.0, 144.5, 144.4, 144.2, 141.6, 141.5, 141.3, 140.9, 139.5, 138.3, 135.4, 134.4, 132.0, 131.4, 130.6, 129.0, 128.7, 128.2, 128.18, 128.14, 128.1, 126.9, −5.6. HRMS: m/z 984.3275 (M^+, calcd 984.4151).

3,4-BTPEMTPS (7). The experimental procedure for the synthesis of this compound is analogous to that described above for the synthesis of 2,5-BTPEMTPS. 3,4-BTPEMTPS was obtained as a greenish yellow solid in 35% yield.

^{1}H NMR (300 MHz, CD_2Cl_2): δ (TMS, ppm) 7.59 (d, 2H, J = 7.2 Hz), 7.35−7.30 (m, 3H), 7.11−7.00 (m, 30H), 6.96−6.93 (m, 6H), 6.86−6.83 (m, 4H), 6.73 (d, 4H, J = 7.8 Hz), 6.55 (d, 4H, J = 8.4 Hz), 0.76 (s, 3H). ^{13}C NMR (75 MHz, $CDCl_3$): δ (TMS, ppm) 156.0, 144.4, 144.3, 142.8, 141.5, 141.3, 140.7, 140.0, 137.7, 135.3, 134.2, 132.1, 132.0, 131.2, 130.5, 130.3, 129.8, 128.9, 128.4, 128.3, 128.2, 127.1, 126.3. −5.7. HRMS: m/z 984.2544 (M^+, calcd 984.4151).

Device Fabrication. The OLED devices were fabricated on glasses coated with 80 nm thick ITO layers with sheet resistance of 25Ω/□. Prior to being loaded into the pretreatment chamber, the ITO-coated glasses were soaked in ultrasonic detergent for 30 min, followed by spraying with deionized water for 10 min, soaking in ultrasonic deionized water for 30 min, and oven

baking for 1 h. The cleaned glasses were treated by perfluoromethane (CF_4) plasma with a power of 100 W, gas flow of 50 sccm, and pressure of 0.2 Torr for 10 s in the pretreatment chamber. The glasses were then transferred to the organic chamber with a base pressure of 7×10^{-7} Torr without breaking vacuum for depositing NPB, BTPEMTPS (or BTPE or BTPEMTPS:BTPE), and TPBi (and Alq_3), which served as hole-transporting, light-emitting, and hole-blocking (and electron-transporting) layers, respectively. The samples were then transferred to the metal chamber for cathode deposition, which was composed of lithium fluoride (LiF) capped with aluminum (Al).

The light-emitting area was 4 mm^2 defined by the overlap of cathode and anode. The current density−voltage characteristics of the devices were measured by the HP4145B semiconductor parameter analyzer. The forward direction photons emitted from the devices were detected by a calibrated UDT PIN-25D silicon photodiode. The L and η_{ext} values of the OLED devices were inferred from the photocurrents of the photodiode. The EL spectra were obtained with a PR650 spectrophotometer. All measurements were carried out under air at room temperature without device encapsulation.

Nanoaggregate Preparation. Stock THF solutions of the luminogens with a concentration of 10^{-4} M were prepared. Aliquots of the stock solution were transferred to 10 mL volumetric flasks. After appropriate amounts of THF were added, water was added dropwise under vigorous stirring to furnish 10^{-5} M solutions with different water contents (0−99.5 vol %). The PL measurements of the resulting solutions or suspensions were then performed immediately.

Acknowledgment. This project was partially supported by the Research Grants Council of Hong Kong (603008 and 601608), the University Grants Committee of Hong Kong (AoE/P-03/08), and the National Science Foundation of China (20634020 and 20974028). B.Z.T. thanks the support from Cao Gaungbiao Foundation of Zhejiang University.

References and Notes

(1) (a) Birks, J. B. *Photophysics of Aromatic Molecules*; Wiley: London, UK, 1970. (b) Capek, I. *Adv. Colloid Interface Sci.* **2002**, *97*, 91. (c) Mancin, F.; Scrimin, P.; Tecilla, P.; Tonellato, U. *Coord. Chem. Rev.* **2009**, *253*, 2150.

(2) (a) Swager, T. M. *Acc. Chem. Res.* **2008**, *41*, 1181. (b) Grimsdale, A. C.; Chan, K. L.; Martin, R. E.; Jokisz, P. G.; Holmes, A. B. *Chem. Rev.* **2009**, *109*, 897. (c) Liu, J.; Lam, J. W. Y.; Tang, B. Z. *Chem. Rev.* **2009**, *109*, 5799.

(3) For recent reviews, see: (a) Hong, Y.; Lam, J. W. Y.; Tang, B. Z. *Chem. Commun.* **2009**, 4332. (b) Liu, J.; Lam, J. W. Y.; Tang, B. Z. *J. Inorg. Organomet. Polym. Mater.* **2009**, *19*, 249. (c) Wang, M.; Zhang, G.; Zhang, D.; Zhu, D.; Tang, B. Z. *J. Mater. Chem.* **2010**, *20*, 1858.

(4) Luo, J.; Xie, Z.; Lam, J. W. Y.; Cheng, L.; Chen, H.; Qiu, C.; Kwok, H. S.; Zhan, X.; Liu, Y.; Zhu, D.; Tang, B. Z. *Chem. Commun.* **2001**, 1740.

(5) (a) Chen, J.; Law, C. C. W.; Lam, J. W. Y.; Dong, Y. P.; Lo, S. M. F.; Williams, I. D.; Zhu, D.; Tang, B. Z. *Chem. Mater.* **2003**, *15*, 1535. (b) Li, Z.; Dong, Y.; Mi, B.; Tang, Y.; Häussler, M.; Tong, H.; Dong, P.; Lam, J. W. Y.; Ren, Y.; Sun, H. H. Y.; Wong, K.; Gao, P.; Williams, I. D.; Kwok, H. S.; Tang, B. Z. *J. Phys. Chem. B* **2005**, *109*, 10061.

(6) Dong, Y. Q.; Lam, J. W. Y.; Qin, A.; Liu, J.; Li, Z.; Tang, B. Z.; Sun, J.; Kwok, H. S. *Appl. Phys. Lett.* **2007**, *91*, 011111.

(7) (a) Yuan, W. Z.; Lu, P.; Chen, S.; Lam, J. W. Y.; Wang, Z.; Liu, Y.; Kowk, H. S.; Ma, Y.; Tang, B. Z. *Adv. Mater.* **2010**. 10.1002/adma.200904056. Published Online: Mar 8, 2010. (b) Hong, Y.; Xiong, H.; Lam, J. W. Y.; Häu*β*ler, M.; Liu, J.; Yu, Y.; Zhong, Y.; Sung, H. H. Y.; Williams, I. D.; Wong, K. S.; Tang, B. Z. *Chem.—Eur. J.* **2010**, *16*, 1232. (c) Li, Z.; Dong, Y. Q.; Lam, J. W. Y.; Sun, J.; Qin, A.; Häu*β*ler, M.; Dong, Y. P.; Sung, H. H. Y.; Williams, I. D.; Kwok, H. S.; Tang, B. Z. *Adv. Funct. Mater.* **2009**, *19*, 905.

(8) Chen, H. Y.; Lam, J. W.; Luo, J. D.; Ho, Y. L.; Tang, B. Z.; Zhu, D.; Wong, M.; Kwok, H. S. *Appl. Phys. Lett.* **2002**, *81*, 574.

(9) Murata, H.; Kafafi, Z. H.; Uchida, M. *Appl. Phys. Lett.* **2002**, *80*, 189.

(10) Zhao, Z.; Chen, S.; Shen, X.; Mahtab, F.; Yu, Y.; Lu, P.; Lam, J. W. Y.; Kwok, H. S.; Tang, B. Z. *Chem. Commun.* **2010**, *46*, 686.

(11) (a) Khabashesku, V. N.; Balaji, V.; Boganov, S. E.; Nefedov, O. M.; Michl, J. *J. Am. Chem. Soc.* **1994**, *116*, 320. (b) Tamao, K.; Ohno, S.; Yamaguchi, S. *Chem. Commun.* **1996**, 1873. (c) Yamaguchi, S.; Tamao, K. *J. Chem. Soc., Dalton Trans.* **1998**, 3693.

(12) (a) Yamaguchi, S.; Endo, T.; Uchida, M.; Izumizawa, T.; Furukawa, K.; Tamao, K. *Chem.—Eur. J.* **2000**, *6*, 1683. (b) Uchida, M.; Izumizawa, T.; Nakano, T.; Yamaguchi, S.; Tamao, K.; Furukawa, K. *Chem. Mater.* **2001**, *13*, 2680. (c) Palilis, L. C.; Makinen, A. J.; Uchida, M.; Kafafi, Z. H. *Appl. Phys. Lett.* **2003**, *82*, 2209. (d) Boydston, A. J.; Yin, Y.; Pagenkopf, B. L. *J. Am. Chem. Soc.* **2004**, *126*, 3724. (e) Lee, J.; Liu, Q. D.; Bai, D. R.; Kang, Y.; Tao, Y.; Wang, S. *Organometallics* **2004**, *23*, 6205. (f) Geramita, K.; McBee, J.; Shen, Y. L.; Radu, N.; Tilley, T. D. *Chem. Mater.* **2006**, *18*, 3261. (g) Liu, Y.; Chen, Z.; Chen, J.; Wang, F.; Cao, Y. *Polym. Bull.* **2007**, *59*, 31. (h) Booker, C.; Wang, X.; Haroun, S.; Zhou, J.; Jennings, M.; Pagenkopf, B. L.; Ding, Z. *Angew. Chem., Int. Ed.* **2008**, *47*, 7731. (i) Aubouy, L.; Huby, N.; Hirsch, L.; van der Lee, A.; Gerbier, D. *New J. Chem.* **2009**, *33*, 1290.

(13) Yu, G.; Yin, S.; Liu, Y.; Chen, J.; Xu, X.; Sun, X.; Ma, D.; Zhan, X.; Peng, Q.; Shuai, Z.; Tang, B. Z.; Zhu, D.; Fang, W.; Luo, Y. *J. Am. Chem. Soc.* **2005**, *127*, 6335.

(14) Vyas, V. S.; Rathore, R. *Chem. Commun.* **2010**, *46*, 1065.

(15) (a) Bulovic, V.; Khalfin, V. B.; Gu, G.; Burrows, P. E.; Garbuzov, D. Z.; Forrest, S. R. *Phys. Rew. B* **1998**, *58*, 3730. (b) Kolosov, D.; Adamovich, V.; Djurovich, P.; Thompson, M. E.; Adachi, C. *J. Am. Chem. Soc.* **2002**, *124*, 9945. (c) Chen, T. R. *J. Mol. Struct.* **2005**, *737*, 35. (d) Zhao, D.; Xu, Z.; Zhang, F.; Song, S.; Zhao, S.; Wang, Y.; Yuan, G.; Zhang, Y.; Xu, H. *Appl. Surf. Sci.* **2007**, *253*, 4025.

(16) Zhao, Z.; Wang, Z.; Lu, P.; Chan, C. Y. K.; Liu, D.; Lam, J. W. Y.; Sung, H. H. Y.; Williams, I. D.; Ma, Y.; Tang, B. Z. *Angew. Chem., Int. Ed.* **2009**, *48*, 7608.

JP910728X